ELSEVIER

Check for updates

Prospects for practical anode-free sodium batteries

Yujie Chen [1], Chao Ye [1], Nianji Zhang, Jiahao Liu, Huan Li, Kenneth Davey, Shi-Zhang Qiao *

School of Chemical Engineering, The University of Adelaide, Adelaide, SA 5005, Australia

Anode-free sodium batteries (AFSBs) with high energy density and cost-efficiency are practically promising for the transition to clean-energy society. However, application is limited because of low coulombic efficiency (CE) and limited cycle-life, together with a lack of understanding in device energy density and cost. Here we report a critical assessment of selected AFSBs with lithium-ion batteries (LIBs) and sodium-ion batteries (SIBs) from energy density and cost perspectives, based on commercial 4680 cylindrical construction. We establish reasons for low cycle-life of AFSBs and summarize current research in AFSBs. We confirm energy density range, materials cost, and potential demand for AFSBs *via* computation based on 4680 battery devices. We show the impact of active sodium ions and cathode active sites on cycle life. We compare the improvements in cycle-life achieved though electrolyte innovation, artificial solid electrolyte interphase (SEI) engineering, current collector modification, and pre-sodiation, along with the resulting energy density. We provide perspectives on likely future research to boost practical application of AFSBs. We conclude that findings will be of benefit in design for anode-free sodium batteries for clean energy storage and of interest therefore to a range of researchers in electrochemistry, materials and device engineering.

Keywords: Anode-free; Sodium battery; 4680 Battery; Energy density; Coulombic efficiency

Introduction

The establishment of a carbon–neutral economy depends on sustainable energy storage, amongst which lithium-ion batteries (LIBs) are widely reported [1–3]. However, a drawback with these is a highly significant growth in demand, together with limited abundance of lithium resources and cost increase [4]. Additionally, an uneven global distribution of critical elements in LIBs including, Li, Co and Ni, has potential for supply chain insecurity [5,6]. Sodium-ion batteries (SIBs) have similar working mechanisms and manufacturing to LIBs, together with elemental abundance and low cost are seen as a practical alternative [7–10]. Significantly, companies including, Build Your Dreams Motors [11], Contemporary Amperex Technology Co., Ltd. [12], Hi Na [13], Faradion [14] and Natron Energy [15], have reported SIBs projects. However, the maximum reported energy density of SIBs is 90–160 Wh kg^{-1}, a value comparable with that of 150–180 Wh kg^{-1} for LIBs with lithium iron phosphate (LFP) cathode [13]. SIBs with higher energy density are therefore of interest, especially in high-demand applications, including electric vehicles (EVs) and stationary storage [16,17].

Anode-free sodium batteries (AFSBs) have attracted significant interest because of high energy density [18,19]. In contrast to LIBs and SIBs with 'intercalation' hosts on the anode side, AFSBs collect sodium ions on the negative electrode current collector *via* forming a compact layer of sodium metal, Fig. 1. Importantly, this anode-free design exhibits higher energy density and has lower cost than SIBs.

* Corresponding author.
E-mail address: Qiao, S.-Z. (s.qiao@adelaide.edu.au)
[1] These authors contributed equally to this work.

1369-7021/© 2024 The Author(s). Published by Elsevier Ltd. This is an open access article under the CC BY license (http://creativecommons.org/licenses/by/4.0/).

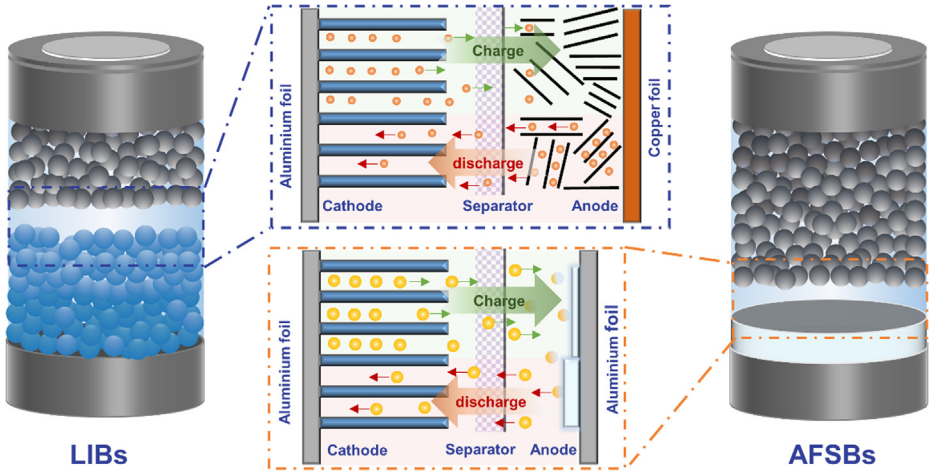


FIG. 1

Working mechanism illustration of LIBs and AFSBs.

However, drawbacks with AFSBs include high chemical activity of sodium metal deposited on the anode collector, large sodium metal volume expansion during charging, and unstable cycling performance. A number of means have been reported to obviate these including electrolyte innovation [20], construction of artificial solid electrolyte interphase (SEI) [21], sodium compensation agent [22] and current collector engineering [23].

In this review we report a critical assessment of selected AFSBs, using a practical 4680 cylindrical battery configuration of high energy density and low cost, and quantitatively compare with LIBs and SIBs. We show the relationship between coulombic efficiency (CE) and cycle life, especially with the impact of active sodium ions and cathode active sites on cycle life. We compare the improvements in cycle-life achieved though electrolyte innovation, artificial SEI engineering, current collector modification, and pre-sodiation, along with the resulting energy density. We provide perspectives on likely future research to boost practical application of AFSBs. We conclude that these findings will be applicable to design for anode-free sodium batteries for clean energy storage and of therefore benefit to a range of researchers and manufacturers.

Energy density of AFSBs and market demand

Battery design and device energy density

Reportedly by removing the anode active material, there theoretically is a significant increase in both volumetric energy density (VED) and gravimetric energy density (GED). However, to exploit this for application, the device-level energy density must be reliably established. GED for example is reportedly widely computed from:

$$\mathrm{GED} = \frac{\mathrm{Capacity} \times \mathrm{Voltage}}{\mathrm{Active\ material\ mass}} \quad (1)$$

in which energy density is based on active material mass. Eq. (1) is a useful means to determine performance for a specific material, however it can be misleading when applied to practical battery at the device-level. For example, the same materials in different battery structures can exhibit varying energy density because of different design [24,25]. Therefore, it is necessary to assess and compare using same battery structure and similar design. With the battery production towards the TWh-level, battery designs are towards unity to decrease production cost and meet recycling needs [26,27]. Amongst reported battery designs, cylindrical, prismatic and pouch, the cylindrical battery is of significant interest, especially the 4680 type battery [28–30]. As an upgraded version of 18650 and 21700 cylindrical batteries for powering EVs, the 4680 battery exhibits greater individual energy, together with the fact of a simplified manufacturing that reduces overall production cost. Its full tab design facilitates 'even current' distribution, aiding in uniform deposition of metal on the negative electrode. The steel casing boosts safety of the metal battery. Therefore the 4680 battery design was selected as a reference to assess GED and VED of different battery systems.

A battery can be considered as the combination of primary working components made from several minimal units, together with auxiliary working components including, electrode tabs, battery casing and overhangs. VED and GED at the device-level is computed from the energy, mass and volume of the primary working components and the auxiliary working components. In design for different battery systems important parameters including, cathode thickness, active material loading ratio and electrode porosity, are set at the same value as for the Tesla 4680 battery. The feature of separator and the current collector in the minimum units are consistent for different battery systems. The major difference between battery systems is in capacity, voltage, initial CE and press density of its active material. Corresponding adjustments are made to the anode based on changes in the cathode and negative electrode to positive electrode ratio (N/P). Because the battery design is set to be consistent, computations are simplified by making total mass of auxiliary working components the same.

Based on this we therefore established the energy, mass and volume of the minimum unit for different battery systems. Because the volume of the primary working components is consistent within a 4680 battery casing, it is possible to determine the total number of minimum units that can be fitted for LIBs, SIBs and AFSBs. The device-level energy density for different battery systems in 4680 configurations can be determined for mass and volume energy density, Fig. 2a.

The computed GED for LIBs with LFP as a cathode and synthetic graphite (Gr) as an anode is seen from the figure to be

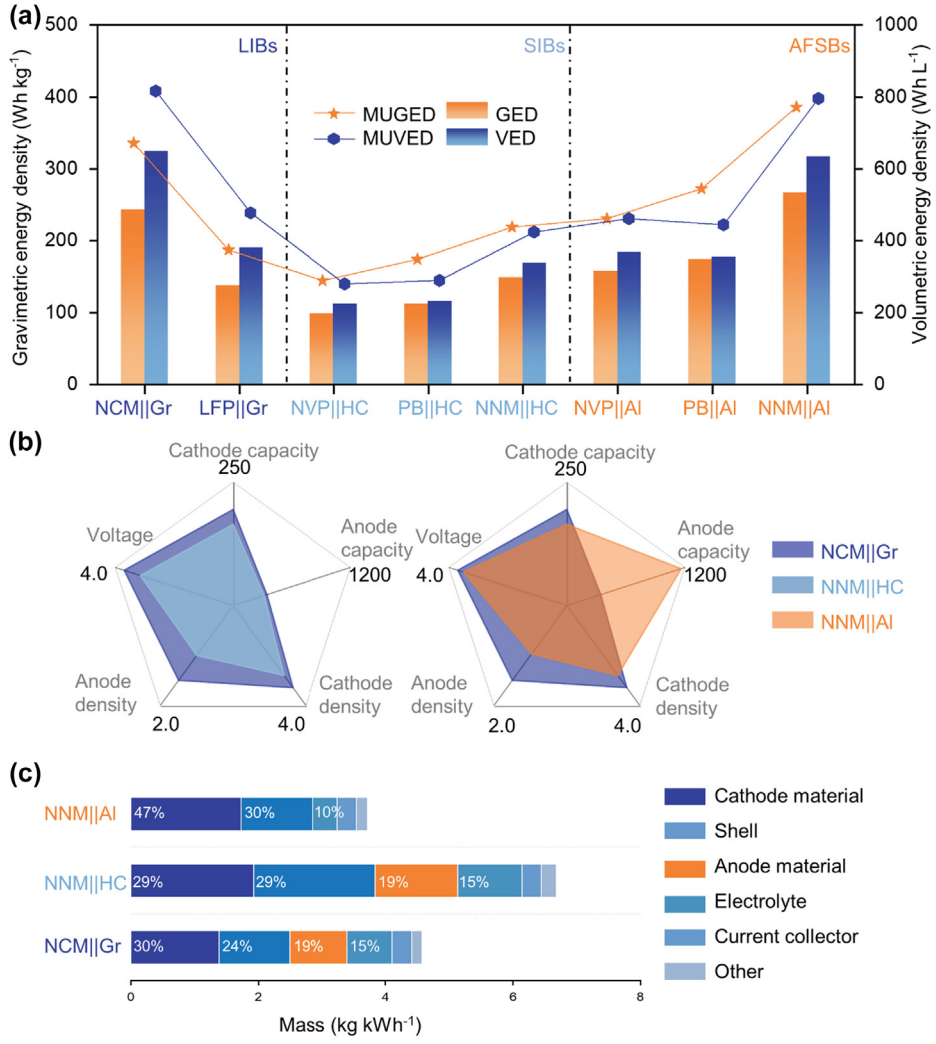


FIG. 2

Device energy density analyses (a) Energy density comparison for LIBs: $LiNi_{0.8}Co_{0.1}Mn_{0.1}O_2$ (NCM)||synthetic Graphite (Gr), LFP||Gr, SIBs: sodium vanadium phosphate (NVP)||hard carbon (HC), Prussian blue (PB) ||HC, P2 type sodium transitional metal oxide (NNM) ||HC, and AFSBs: NVP|| Al, PB||Al, NNM||Al. (b) Parameter analysis for energy density and (c) Device mass distribution for NCM||Gr, NNM||HC, and NNM||Al.

ca. 140 Wh kg^{-1}, a value that agrees well with reported data for LFP batteries [31,32]. For SIBs three types of cathode were computed for, namely, sodium superionic conductor compound [33], Prussian blue analogues [34] and sodium transitional metal oxides [35], combined with a hard carbon (HC) anode [36]. Value for GEDs was determined to be 100–150 Wh kg^{-1} and, importantly, consistent with reported data for SIBs [37–39].

It is concluded therefore that the computational method is reliable.

It is apparent that GED and VED for SIBs are significantly lower than those for LIBs. Compared with LIBs using $LiNi_{0.8}Co_{0.1}Mn_{0.1}O_2$ (NCM) as a cathode, GED and VED for SIBs is *ca.* a half. This arises from differences in capacity, voltage and real density of cathode and anode materials. The radar chart of Fig. 2b comparatively summarizes SIBs using P2-$NaNi_{0.33}Mn_{0.66}O_2$ (NNM) [40] as cathode paired with HC anode over LIBs using NCM as cathode pairing Gr as the anode. The cathode capacity for NNM exhibits just 84.6 % of NCM, the anode capacity of HC is just 91.3 % of Gr and the full-cell voltage is just 85.1 %. Additionally, because of lower density of the cathode and anode materials, the number of minimum units within the device is just 87.2 % compared with LIBs, resulting in a lower energy density, Table 1. To obviate influence of battery structural design, the 4680 might not be optimal for SIBs, minimum unit volumetric energy density (MUVED) and gravimetric energy density (MUGED) were computed using the following equation and plotted for selected chemistry, Fig. 2a:

$$\mathrm{MUGED} = \frac{\mathrm{Capacity}_{\mathrm{MUs}} \times \mathrm{Voltage}}{\mathrm{Mass}_{\mathrm{MUs}}} \quad (2)$$

$$\mathrm{MUVED} = \frac{\mathrm{Capacity}_{\mathrm{MUs}} \times \mathrm{Voltage}}{\mathrm{Volume}_{\mathrm{MUs}}} \quad (3)$$

where "$\mathrm{capacity}_{\mathrm{MUs}}$" refers to the reversible capacity in the minimal units (MUs), by taking the N/P ratio and the initial CE of the cathode and anode material into consideration. "Voltage" represents the nominal voltage during discharge. "$\mathrm{Mass}_{\mathrm{MUs}}$" and "$\mathrm{Volume}_{\mathrm{MUs}}$" denote the total mass and volume of the MUs. MUVED and MUGED are the VED and GED for an infinitely expanded casing i.e., the volume

and mass ratio of the auxiliary components can be ignored. However, in computed SIBs system the mass and volume energy density for the minimum unit are less than for currently used NCM||Gr chemistry. Therefore to boost the energy density of SIBs innovation is needed at material and chemical system level.

With AFSBs, sodium metal deposited on the negative electrode during charging exhibits a higher specific capacity of 1165 mAh g^{-1} and a lower potential of 0 V *vs*. Na^+/Na. The density of sodium metal is similar to the press density of sodium-intercalated hard carbon. Compared with SIBs, the GED for AFSBs chemistry was found to increase by *ca*. 61.4 %, 55.5 % and 79.6 %, respectively, and VED increased by *ca*. 65 %, 53.6 % and 87.6 %, respectively, in three representative cathode materials sodium vanadium phosphate (NVP), Prussian blue (PB) [41] and NNM. With high energy density cathode materials, the anode-free design has a greater impact on boosting energy density. The reason is that cathode materials are primary contributors to capacity and voltage. The presence of large amount anode material reduces the device-level energy density discrepancy caused by differences in cathode materials. Therefore, in anode-free systems the performance of high energy density cathode materials exhibits significant increase. As is seen in Fig. 2a, the energy density for AFSBs with NNM as cathode slightly exceeds LIBs with NCM as cathode.

The radar chart of Fig. 2b evidences that whilst parameters for NNM||HC remain less than those for NCM||Gr, the high-capacity sodium in the anode-free configuration significantly exceeds Gr and reduces the minimal unit volume to permit additional minimum units to be accommodated in the 4680 casing, and an increase in energy density.

To better understand the energy density contribution of different components, a mass comparison was determined on a per kWh basis, Fig. 2c. The cathode mass in NNM||Al AFSBs accounts for *ca*. 46.6 % of total mass, significantly exceeding the *ca*. 30.3 % for NCM in NCM||Gr LIBs. Incorporating additional cathode materials into a single battery gives a higher battery capacity, compensating for intrinsic shortcomings of NNM materials in specific capacity, voltage and density. *Via* removal of anode material, representing *ca*. 28.7 % of the mass in NNM||HC, overall battery mass is significantly reduced. Electrolyte usage in AFSBs also decreases because the dense sodium deposition in negative electrode lacks pores to retain electrolyte. The anode-free design is therefore a better design to boost energy density of SIBs.

With incorporation of three sodium battery cathode materials namely, NVP, PB and NNM, into AFSBs, the device-level GED values are, respectively, 159, 176 and 269 Wh kg^{-1}. Correspondingly, VED values are 370, 357 and 638 Wh L^{-1} (Table 1). These values cover the energy density range from LFP||Gr to NCM||Gr. AFSBs therefore can be used to substitute current energy storage devices using LIBs.

With more battery manufacturers producing 4680 cylindrical batteries [42,43]. AFSBs with VED and GED similar to LIBs stand a strong chance to replace current LIBs in various applications without the need for excessive module or pack adjustments.

Potential demand for AFSBs

Cost of a battery is important in determining application. Importantly, low cost of AFSBs stems from, (1) low manufacturing costs, (2) stable and simplified supply chain, and (3) inexpensive raw materials [37,44–46]. Based on reported increase in LIBs production, battery technologies that require significant changes to existing production-lines, together with additional capital investment, will not be attractive to manufacturers [47,48]. An important benefit of AFSBs is compatibility with current LIBs production, eliminating need for additional equipment, or process developments [49]. Additionally, *via* eliminating the anode,

TABLE 1

Device energy density computation data for LIBs (NCM||Gr, LFP||Gr), SIBs (NNM||HC, NVP||HC, PB||HC) and AFSBs (NNM||Al, NVP||Al, PB||Al) in 4860 battery geometry.*

Battery type	NCM||Gr	LFP||Gr	NNM||HC	NNM||Al	NVP||HC	NVP||Al	PB||HC	PB||Al
Cathode material	NCM	LFP	NNM	NNM	NVP	NVP	PB	PB
Cathode area capacity (mAh cm^{-2})	5.2	2.8	3.7	3.7	1.7	1.9	1.8	1.8
Cathode specific capacity (mAh g^{-1})	195	143	165	165	102	112	147	150
Cathode coating mass (mg)	27.7	20.8	23.2	23.2	17.4	17.4	12.5	12.5
Cathode press density (g cm^{-3})	~3.3	~2.5	~2.8	~2.8	~2.1	~2.1	~1.5	~1.5
Anode area capacity (mAh cm^{-2})	5.5	3.0	4.3		1.8		1.9	
Anode specific capacity (mAh g^{-1})	345	345	315	1165	315	1165	315	1165
Anode coating mass (mg)	16.8	9.0	14.2		6.1		6.3	
Anode press density (g cm^{-3})	~1.5	~1.5	~1.0	0.97	~1.0	0.97	~1.0	0.97
Total electrolyte mass (g)	36.5	48.2	36.3	25.8	35.7	30.2	35.7	30.1
Average voltage (V)	3.70	3.10	3.15	3.50	3.05	3.40	3.09	3.44
Total capacity (Ah)	23.4	16.4	14.4	24.3	9.8	14.5	10.0	13.8
Total energy (Wh)	86.4	51.0	45.2	84.9	29.8	49.2	30.9	47.4
Total mass (g)	355	368	302	316	302	309	273	270
GED (Wh kg^{-1})	243	139	150	269	99	159	113	176
VED (Wh L^{-1})	650	383	340	638	224	370	232	357
Number of MUs	4452	5900	3882	6554	5711	7681	5644	7648
MUGED (Wh kg^{-1})	333	187	219	386	145	231	174	272
MUVED (Wh L^{-1})	810	478	424	796	280	461	290	445

* Active material loading is 96 % in all electrodes. Current collector is 13 μm Al except LIBs anode where 6 μm Cu is used as current collector. Electrode porosity is *ca*. 30 to 40 %. Gr with initial CE of ca. 93 % and HC with initial CE of *ca*. 90 % were used as an anode material for LIBs and SIBs, respectively. The initial CE of cathode materials is *ca*. 89 %, 95 %, 83 %, 98 %, 91 % for NCM, LFP, NNM, NVP and PB, respectively. Separator with *ca*. 40 % porosity and *ca*. 1 mg cm^{-2} is selected for all batteries. Total volume of 4680 casing is *ca*.133 mL.

traditional anode production including, mixing, coating, drying and calendaring, can be omitted from AFSBs manufacturing to significantly reduce production cost and boost production yield and efficiency [50,51].

An additional cost advantage with AFSBs is simplification of the battery supply chain i.e. (1) use of Al-foil with high-production capability for both anode and cathode current collectors reduces material costs and simplifies Bill of Materials [52], and (2) compared with lithium-based materials, the raw materials for sodium-based materials are widely available and are more evenly distributed globally. Supply chain price fluctuation, perhaps because of geopolitical tension, is therefore reduced [6,53,54].

A significant cost advantage however is in materials level. To establish this, the relatively high energy density, commercialized $NaNi_{0.4}Fe_{0.2}Mn_{0.4}O_2$ (NFM) was selected as the cathode material for SIBs and AFSBs. The material cost per kWh for SIBs using NFM||HC is seen to be greater than that for LIBs using NCM||Gr, despite that material cost for NFM is just 61.7 % of that of NCM by mass of US$ 16.6 k *vs*. US$ 26.9 k per tonne. This is because to exhibit equivalent energy the quantity of cathode material required for SIBs is *ca*. 2 times compared with that for LIBs. On the anode side the cost for HC is currently 2.5 times greater than that for Gr of US$ 20.1 k *vs*. 8.0 k per tonne. Additionally, use of HC per kWh in SIBs is 52.2 % greater than that for graphite per kWh in LIBs. These are major reasons contributing to high cost of existing SIBs. Sodium battery materials are likely to enter into large-scale production. It is likely that with large-scale production sodium battery materials will exhibit price decreases in parallel with lithium battery materials of recent decades [55–57].

AFSBs exhibit cost advantage with current material price, Fig. 3a. It can be seen from the figure that material cost per kWh for AFSBs is US$ 48.1, which is *ca*. 84.5 % that for NCM||Gr and 54.1 % that for NFM||HC. This cost advantage results from elimination of active material on the anode that accounts for *ca*. 31 % of cost in SIBs and 12.7 % in LIBs.

Without the influence of HC, the anode-free full-cell operates at a higher voltage, reducing the cathode material use to US$39.3 that is similar to LIBs of US$37.3, and more cost-effective when compared to SIBs of US$48.5. AFSBs exhibit electrolyte cost benefit in two areas, namely the: (1) adoption of affordable sodium salts reduce electrolyte cost to US$ 2.7 k per tonne, some 39.2 % of cost for LIBs electrolyte, and (2) dense deposition of sodium at the anode reduces overall demand for electrolyte per kWh to *ca*. 0.5 kg some 75.4 % compared with NCM||Gr LIBs, resulting in *ca*. 6.2 % reduction in cost. Additionally, substituting 13 μm Al-foil for 6 μm Cu-foil reduces current collector cost by *ca*. 44.5 % and contributes to *ca*. 2.7 % of overall cost. The cost for components including separator, binders and conductive agents is similar to that for LIBs.

It is evident that in all these battery systems, the cathode is the primary cost. However in the case of AFSBs, cost of the cathode accounts for *ca*. 81.5 % of the total material cost. In parallel with device-level energy density, where the presence of anode material can reduce the discrepancy caused by the differences in cathode material. The presence of the anode material can also reduce the cost discrepancy caused by cathode materials in device-level. This finding evidences that in production, manufacturers choosing NCM||Gr LIBs or NFM||HC SIBs will need to allocate increased research resources to both cathode and anode materials, and conversely, manufacturers of AFSBs will boost profit at device-level by concentrating solely on cathode material cost-reductions.

The potential market demand was established *via* quantitatively comparing different electrochemical energy storage batteries with reported energy density, together with global markets, Fig. 3b. It was apparent that the present market is dominated by LIBs with VEDs in the range 350–650 Wh L^{-1} and GEDs of 150–250 Wh kg^{-1} [58,59]. Because most LIBs are used in EVs, strict requirements are applied in minimal VED, limiting replacement from other battery technologies [60,61]. Achieving such energy density with SIBs requires innovation at material level and also 'breakthroughs' in battery technology. However, with design similar to that for 4680 battery, AFSBs exhibit VED for EVs. Removal of anode material makes GED for AFSBs slightly higher than for LIBs, Fig. 3b. This could provide a 'smooth' transition from existing LIBs systems to AFSBs. Additionally, traditional lead-acid batteries with VED in the range 60–110 Wh L^{-1} and GED 40–60 Wh kg^{-1} have a present significant market compared with nickel–cadmium batteries (Ni-Cd) and nickel metal hydride battery (Ni-MH). However, practical environmental problems with lead-acid batteries significantly hinders development. Based on reported forecast (from Global Data) the market for lead-acid batteries will not increase meaningfully for the foreseeable period, resulting in a market decrease [62]. Because material cost for AFSBs is approaching the cost for lead-acid batteries, it is concluded that AFSBs will therefore emerge as strong contenders in lead-acid battery market.

Long-cycle AFSBs

Despite significant advantages of AFSBs in energy density and potential for future market demand, three factors delay application including: (1) poor cycling performance, (2) volume change within cycling, and (3) safety [19,49,63]. Volume change during charge and discharge are not exclusive to AFSBs because batteries using metal anode or high-capacity materials can have this problem. Obviating this requires development of 3D current collectors with a fixed electrode thickness, or design of deformable battery casings, coupled with a battery management system to achieve constant-pressure modules. The use of sodium metal raises risks to safety, however, safety of AFSBs is relatively 'good' because (1) battery manufacturing does not involve sodium metal, significantly boosting manufacturing safety, (2) the active sodium ions can be stored in the cathode in discharged state making 0 V battery transport and storage available, and; (3) the sodium metal in the negative electrode comes entirely from the positive electrode material in charge state. Therefore compared with sodium metal batteries with excess sodium metal in the negative electrode, safety of AFSBs is significantly boosted. Additionally, AFSBs operate at a relatively low voltage of 3.5 *vs*. 3.7 V for LIBs. Although this reduces energy density, it boosts safety. The 'soft' nature of sodium metal makes it more readily blocked at the negative electrode by the modified separator. Developing high-safety separators or separator coating materials, or using

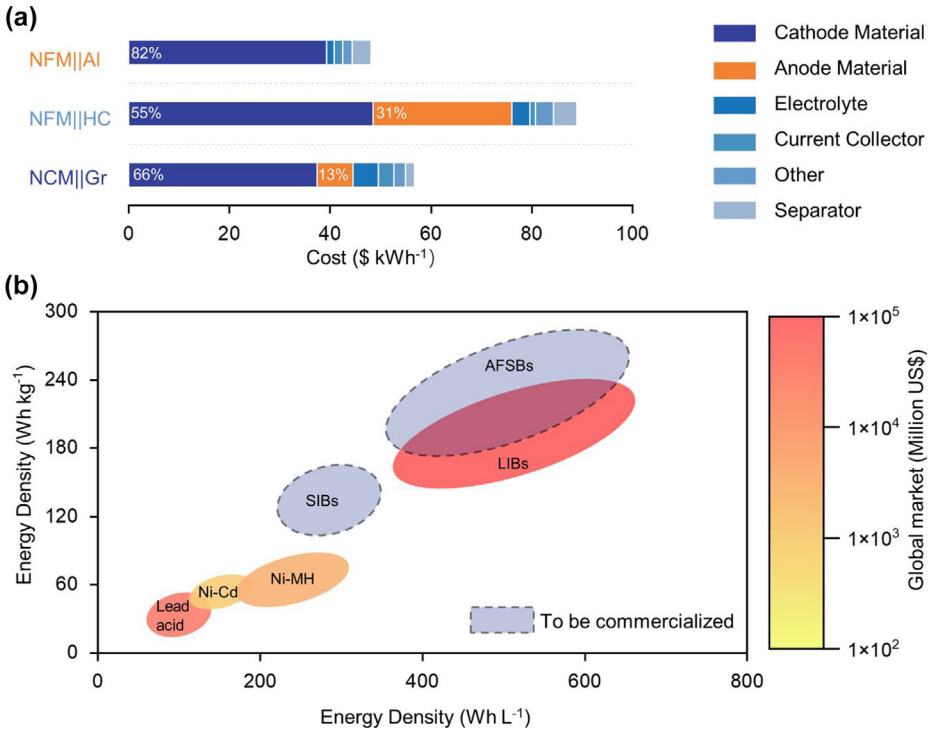


FIG. 3

Material cost and market analysis (a) Comparison of cost in LIBs (NCM||Gr), SIBs (NFM||HC) and AFSBs (NFM||Al). (b) Energy density exhibited and market for battery technologies.

solid-state electrolytes, can boost safety of AFSBs. In addition, the use of a steel casing, such as the 4680 battery design, significantly boosts safety of individual cells. Therefore problems of safety and volume change can be practically addressed. However, if the poor cycling performance is not solved initially at laboratory-scale, AFSBs may not even have an opportunity for industrialization. CE is widely reported as a quantitative measure to evidence battery cycling life [64–67]. An understanding of the relationship between CE and cycling-life is therefore practically useful.

Electrons circulate in the external circuit are detected and recorded *via* testing equipment as capacity. Sodium ions migrate within the internal circuit together with electrons to maintain charge conservation. The number of electrons in the external circuit is reasonably assumed to be equal to the number of sodium ions circulating within the battery. In positive electrode, active material provides active sites to host sodium ions, whilst in the negative electrode, sodium ions convert to deposited metal. Battery CE is defined as the discharge capacity divided by the charge capacity and can therefore be written as:

$$\text{Battery CE}_n = \frac{\text{Disharge capacity}_n}{\text{Charge capacity}_n} = \frac{e^- \text{ back cathode}_n}{e^- \text{ leave cathode}_n} = \frac{Na^+ \text{ back cathode}_n}{Na^+ \text{ leave cathode}_n} \quad (4)$$

Capacity retention refers to the number of completed cycles before the battery capacity decreases to a pre-defined value from its initial. To reach the maximum energy density, the cathode material needs to exhibit full capacity in AFSBs. Therefore, the first-cycle cathode reversible capacity is used as a reference for capacity decay. Capacity retention is expressed as the discharge capacity of the n^{th} cycle divided by the number of cathode active sites of the first cycle, namely:

$$\text{Capacity retention}_n = \frac{\text{Discharge capacity}_n}{\text{Discharge capacity}_1} = \frac{\text{Discharge capacity}_n}{\text{Cathode reversible capacity}_1} \quad (5)$$

In an 'ideal' battery there are no side reactions at either the cathode or anode. Sodium ions released from the cathode during charging fully return to the cathode on discharging, and the cathode exhibits sufficient active sites to host active sodium ions, resulting in a theoretical Battery CE of 100 %. Under these circumstances, the battery exhibits infinite cycling without capacity decay. However, ideal conditions are not practical. In a practical battery there are side reactions in both the cathode and anode that make for a 'complex' Battery CE. Some side reactions cause active sodium ion loss, whilst others cause cathode active-site loss.

Battery CE and capacity retention are defined, respectively, as follows:

$$\text{Battery CE}_n = \frac{\min\left(\text{Active } Na^+{}_n,\ \text{cathode } Na^+ \text{ site}_n\right)}{Na^+\text{leave cathode}_n} \quad (6)$$

$$\text{Capacity retention}_n = \frac{\min\left(\text{Active } Na^+{}_n,\ \text{cathode } Na^+ \text{ site}_n\right)}{\text{Cathode reversible capacity}_1} \quad (7)$$

The lower value between the number of active sodium ions and the number of active sites determines Battery CE and capacity retention.

To establish the impact of active sodium ion loss on Battery CE and capacity retention, a battery with an ideal cathode paired with a practical anode is assumed. Using the ideal cathode in this battery, the number of cathode active sites will be equal to the number of sodium ions at the initial state, and remain constant in following cycles, namely:

$$\text{Cathode reversible capacity}_x = \text{Na}^+ \text{ leave cathode}_x = \text{Cathode active site}_x \quad (8)$$

and every sodium ion embedded in the cathode during discharge 'smoothly' leaves the electrode without losses, namely:

$$\text{Na}^+ \text{ back cathode}_n = \text{Na}^+ \text{ leave cathode}_{n+1} \quad (9)$$

When cycling this battery with appropriate voltage, sodium ions nucleate and grow into metallic sodium on the negative electrode. Any side reactions between the deposited sodium and the electrolyte cause losses of active sodium ions, leading to capacity consumption in each cycle. Assuming that the deposition behaviour of metallic sodium is similar in each cycle, sodium ion loss in each cycle will be proportional to cycling flux. Battery CE becomes a constant value and equals active ions cycling CE (CE_{ion}) i.e.

$$\text{Battery CE} = CE_{ion} = \frac{\text{Na}^+ \text{ back cathode}_1}{\text{Na}^+ \text{ leave cathode}_1} = \frac{\text{Na}^+ \text{ back cathode}_n}{\text{Na}^+ \text{ leave cathode}_n} \quad (10)$$

The relationship between capacity retention rate and CE_{ion} is therefore:

$$\text{Capacity retention}_n = \text{Active ion retention}_n = CE_{ion}{}^n \quad (11)$$

From Eq. (11) the significant impact of the CE_{ion} on cycle-life is apparent.

Assuming a 70 % capacity retention as the end-of-life criterion, the battery performance decreases significantly fast to 70 % after 7 cycles with a CE_{ion} = 95 %, Fig. 4a. When the cycling efficiency is improved from 95 % to 99 %, the cycle life increases significantly from 7 to 36 cycles, respectively. However, despite CE_{ion} = 99.9 %, just 357 cycles can be maintained. To establish a competitive cycling life >1000 cycles, an increase in CE_{ion} to 99.965 % is needed. To boost battery lifespan, it is therefore apparent to increase CE_{ion}. This involves reducing any parasitic reactions between deposited sodium and electrolyte at the negative electrode. The best design therefore is an electrolyte that does not react with sodium, alternatively, boost deposition behaviour of sodium ions at the negative electrode to form a uniform and dense deposition layer that reduces contact area between metallic sodium and the electrolyte. The decreasing of area currents and construction of a sodiophilic-layer are used for a dense deposition. A 3D anode structure is constructed to assuage local current density, and a sodiophilic-layer used for uniform deposition to therefore boost cycling life of AFSBs.

It is reported that during the first deposition of sodium on the negative electrode, a SEI passivation layer needs to be formed, and this layer acts as a protective layer to prevent reactions between highly reactive metallic sodium and electrolyte [68]. However, this reportedly leads to significant loss of active sodium ions because during charging the entire negative electrode is at a similar potential to metallic sodium. A SEI layer forms therefore everywhere the electrode and the electrolyte contacts and causes highly significant active sodium ions loss [69].

Additionally, because all sodium ions in AFSBs originate from the cathode, consumption associated with initial formation of the SEI layer results in a significant impact on capacity retention. Therefore capacity retention is given by:

$$\text{Capacity retention}_n = \text{Active ion retention}_n = ICE_{ion} * CE_{ion}{}^{n-1} \quad (12)$$

where the ICE_{ion} represents the initial active sodium ion coulombic efficiency.

The effect of ICE_{ion} on capacity retention is presented as Fig. 4b. When ICE_{ion} decreased to 95 %, a battery that was originally estimated to last for 357 cycles with an ICEion of 99.9 % cycles for a reduced number of 307 cycles. If ICE_{ion} decreases further to 75 %, the cycle-life of the battery will be just 70 cycles. Therefore, amelioration strategies, including 3D current collectors and high surface area sodiophilic coating, will involve a pre-formation of SEI in a half-cell configuration paired with metallic sodium to compensate for sodium ion losses. Pre-cycling with half-cell significantly increases the production cost for AFSBs.

The change of active sites during battery cycling and its influence on Battery CE and capacity retention are important. When the active sodium ions inside the battery are sufficient, the loss of active sites is controlling of Battery CE and capacity retention. This resembles closely the half-cell when pairing a practical cathode with a sodium chip. The cathode active site loss also positively correlates with cycling flux rate, similar to active sodium ions loss. Irreversible active site loss usually occurs in charging; therefore, the number of active sites is the same in discharge and next charge. The establishment of the cathode active site retention after it stabilizes is given by:

$$\text{Active site retention}_n = CE_{site}{}^{n-1} \quad (13)$$

in which CE_{site} denotes cycling cathode site coulombic efficiency. The capacity retention of the full-cell uses the first cycle cathode reversible capacity as a reference that mitigates impact of the initial cycle active sites change.

In combining the change of active sodium ions and active site, the battery cycling in practice can therefore be simulated. For most cathode materials, after contributing sodium ions in the initial charge, irreversible structural changes result in deactivation of active sites in the cathode. If the 'excess' sodium ions are not able to compensate for the active sodium ions loss from SEI formation in the negative electrode, the battery retention curve is as shown in Fig. 4b (with a different starting point). However, if excess sodium ions number greater than SEI formation sodium ions loss, it remains at the anode as deposited sodium. In SIBs this causes metallic sodium deposition on the anode surface and leads to battery failure [70]. However in AFSBs, these active sodium left at the anode stabilize the SEI film, obviating reactive nucleation during each charge and boost stability of CE_{ion} of the battery.

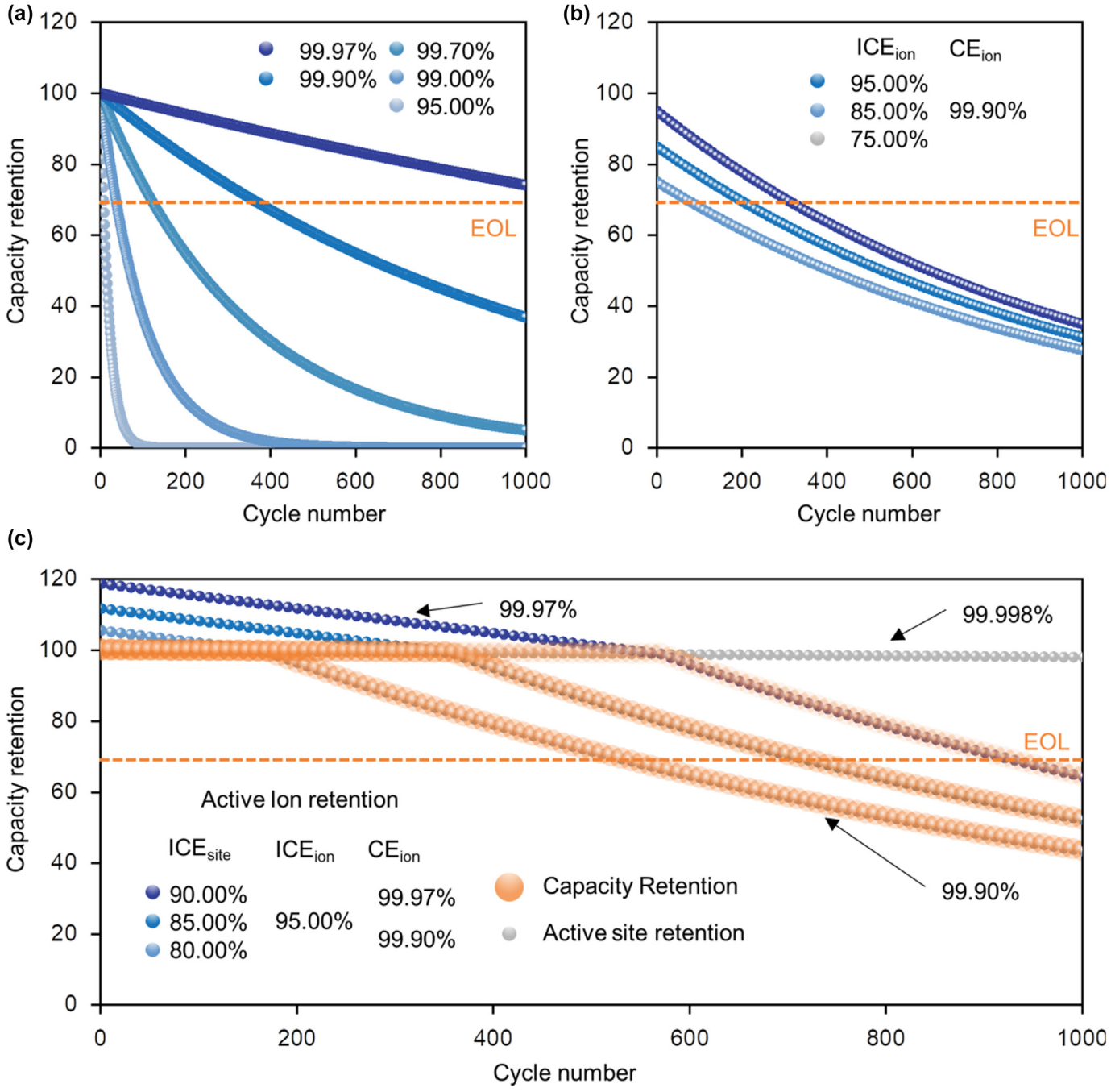


FIG. 4

Simulated capacity retention curve for AFSBs. (a) 'Ideal' cathode||practical anode with CE_{ion} of 95 %, 99 %, 99.7 %, 99.9 % and 99.97 %, respectively. (b) Ideal cathode||practical anode with CE_{ion} = 99.9 % and ICE_{ion} = 95 %, 85 % and 75 %, respectively. (c) Practical battery with active sites cycling CE (CE_{site}) = 99.998 % and active site initial coulombic efficiency of 90 %, 85 %, and 80 %, respectively, and ICE_{ion} = 95 %, CE_{ion} = 99.97 % and 99.9 %.

To better understand, a battery using cathode material with active site retention of 99.998 % and different active sites initial CE of 90 %, 85 % and 80 %, respectively, was developed. The number of active ions change was 95 % ICE_{ion} and 99.9 % CE_{ion}. The simulated battery cycling curves are presented as Fig. 4c, where for example, if the irreversible active sites change on the cathode during the first charge is 90 %, the cathode will exhibit an additional 11.11 % active sodium ion. This is sufficient to compensate for the active sodium ions loss and provide *ca.* 5.5 % active sodium ions deposited on the negative electrode. Importantly, the sodium metal at the negative electrode stabilises the SEI resulting in a boosted CE_{ion} from 99.9 % to 99.97 %, Fig. 4c. Additionally, before the sodium on the negative electrode is consumed, battery retention is controlled by active site retention, allowing it to fully utilize the cathode's capacity and voltage. Active sodium ions inside the battery are continuously depleting, and the active ion consumption in n^{th} cycle can be computed as cathode reversible $capacity_1 \times 99.998\ \%^{n-1} \times (1–99.97\ \%)$. The corresponding curve is presented as Fig. 4c. When the extra sodium is consumed the battery

exhibits degradation similar to that of Fig. 4a, b. Because each charge involves a high-reactivity nucleation, CE_{ion} changes to 99.9 % and becomes controlling of battery lifespan. Despite that there remain active sites, they do not contribute to the capacity of the battery. With excess active sodium ions, the cycling life extended to 522 cycles i.e. >3 times compared with the original number of 173 cycles. If the irreversible active sites change on the cathode during the first charge is 80 %, the cycle life will be increased to 917 cycles. It is concluded that development of cathode materials needs sodium-rich cathode materials, or pre-sodiation agent(s), to provide more active sodium ions.

Based on simulations it is concluded therefore that the rationale to improve cycle life of AFSBs is to boost active ion cycling coulombic efficiency (CEion) via electrolyte optimization and anode current collector modification. Additionally, reducing active sodium ions loss in the initial SEI formation is important, and can be done via pre-establishing an artificial SEI layer, or using electrolyte additives, together with using sodium-rich cathode materials or pre-sodiation materials as additives to give extra active sodium ions.

Recent developments in AFSBs

Optimized electrolyte & artificial interfaces

Extended life and high energy density in AFSBs is determined by maintaining high voltage cathode materials with exceptional capacity retention. However, practical problems are low chemical and mechanical stability of SEI [71] that lead to interfacial reconstruction [72].

In addition, unmodified electrolytes do not provide a suitable electrochemically stable window (ESW) for high voltage cathodes, limiting energy density. Complex reactions between interfaces and electrolyte result in uneven sodium deposition, sodium dendrite growth and active sodium metal losses, which decrease performance of AFSBs. However, optimizing electrolyte composition, including salt, solvent and additives, can be used to obviate these [73]. Optimization is from formation of thin, highly ionic conductive and mechanically robust SEI interfaces. Manipulation of the solvation structure of electrolytes *via* tailored artificial interfaces of selected size [74] and bonding strategies [75] can be used to boost long life and high energy density.

AFSBs with optimized electrolyte and artificial interfaces with boosted cycling performance and high energy density are presented as Fig. 5a. The ordinate (*y-axis*) is the minimum unit energy density at the beginning and end of cycle, the abscissa (*x-axis*) number of cycles (selected cycles before capacity decay > 70 % if the capacity retention more than 70 %), and the width shows different cycling rates.

The 'ideal' solvent for AFSBs is characterized by (1) an elevated, lowest unoccupied molecular orbital (LUMO) and lowered highest occupied molecular orbital (HOMO) level to establish a wide ESW, (2) a rationalized solvation structure for modulating interface component distribution and increasing ion migration rate, and (3) avoidance of high viscosity, ultra-high concentration and costly components to prevent reduced energy density, increased costs, and unfavourable commercial implications.

Ester-based solvents with desirable HOMO level(s) for oxidative resistance and compatibility with high voltage cathodes are commonly used in LIBs and SIBs. However, they are not directly suitable for AFSBs because of a heightened reactivity with deposited sodium layers, resulting in undesired parasitic gases including hydrogen and carbon dioxide [72]. In contrast, ether-based solvents including dimethyl ether (G2), tetraethylene glycol dimethyl ether and diethylene glycol dimethyl ether, reportedly exhibit significant reductive stability on the negative electrode with stable, compact SEI interfaces [20,72,76,77]. Susceptibility to oxidation however leads to cathode electrolyte interface (CEI) reconstruction on the cathode side, contributing therefore to reduced cycle-life in AFSBs. Significantly, limited solubility of ether solvents prevents a concentrated electrolyte being established to enhance cathodic oxidative stability. Therefore, optimizing AFSBs electrolyte components will need to be based on improving ESW and in fostering formation of stable CEI and SEI interfaces.

Boron salts including, $NaBF_4$, Na^+ $[HCB_{11}H_{11}]^{1-}$, are reportedly favourable for B—O and B—F decomposition products to stabilize SEI and CEI and enlarge ESW [20,76,77]. Li et al. reported a dual-salt system of 0.9 M $NaPF_6$ + 0.1 M $NaBF_4$ in G2 as an electrolyte in sodium vanadium (III) fluorophosphate (NVPF)||C@Al that exhibited a high initial energy density of 205 Wh Kg^{-1} [20], Fig. 5b. The inferior solubility of boron salt in G2 leads to a 'relatively' reduced concentration. Compared with pure $NaPF_6$ salt the dual-salt system exhibits elevated LUMO and HOMO determining the stratified structure of SEI and CEI, Fig. 5b. Boron species are strategically dispersed across the outer SEI layer and the inner CEI layer in a 3D arrangement. This unique configuration leads to formation of an ion-conductive channel in the 10 nm thick SEI and a 3 nm thick CEI that protects the high voltage cathode material from dissolution. Consequently, this modification in electrolyte aids the high energy density full-cell to exhibit a long cycling life of >260 cycles with 80 % capacity retention. Tomich et al. reported a weak-coordination method between large anion cluster $[HCB_{11}H_{11}]^{1-}$ and sodium ion to increase ion migration, exhibiting SEI with a significant conductivity of 7.58 mS cm^{-1} [77]. Devoid of fluorine, this method reportedly obviated generation of fluorine-containing anion decomposition products such as HF, to boost cycling stability.

Incorporation of electrolyte additives reportedly can be used to optimize the SEI film *via* modulation of the ratio and range of inorganic constituents [73]. The introduction of 'modest' amounts of fluoroethylene carbonate additives synergistically interacts with $NaPF_6$ salt to exhibit a SEI film comprising internal Na_3PO_4 and external amorphous NaF. This change in architecture obviates SEI cracking and reconstruction caused *via* fragility of organic species on external SEI.

Artificial interface engineering can reportedly be used to boost cycling stability and energy density, as evidenced in Fig. 5c. Whilst extended cycling can be practically achieved *via* HOMO-LUMO design, the balance between organic and inorganic layers in a typical double-layer SEI structure is a continuing present problem.

The artificial interface reported by Wang et al. using a formate-treated Cu-foil to form HCOONa SEI film results in a lower ion migration barrier similar to the organic layer and the dense and ordered configuration characteristics of the inorganic layer [75]. In this method an SEI is formed with a Young's mod-

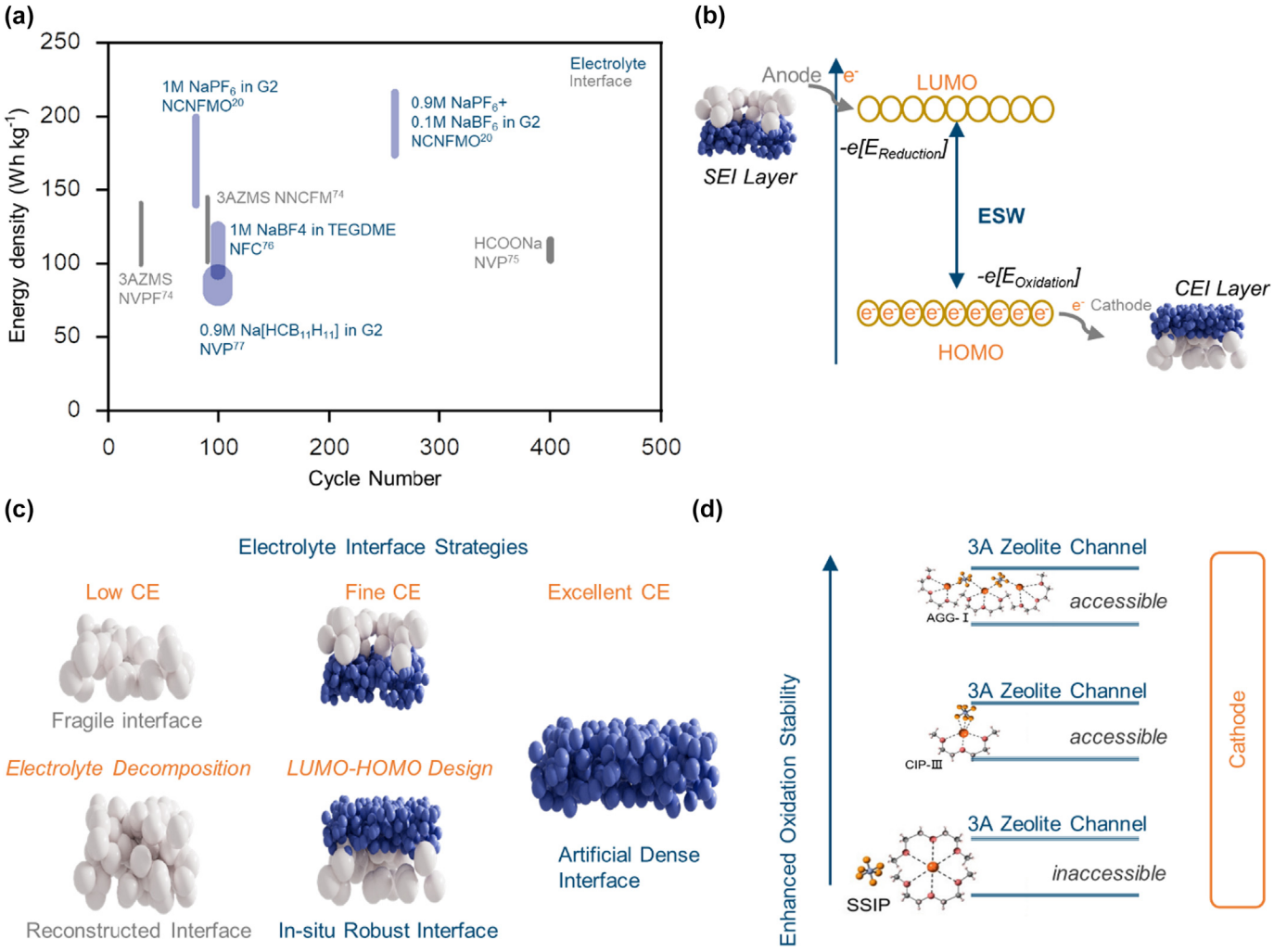


FIG. 5

Developments in electrolyte and artificial SEI. (a) Metrics for lifespan and energy density with electrolyte and interface strategies [20,74–77]. (b) SEI and cathode electrolyte interface (CEI) stratified structure induced via molecular orbital mechanism. (c) Evolution of electrolyte interfaces. Unmodified, in-situ modified, and artificially modified, strategies. (d) Sieving effect induced solvation structures [74].

ulus of 4.3 GPa. XPS etching established the dominant contribution of sodium formate to the SEI, as was evidenced by diminished presence of C—O—C, C—C, and O—P=O bonds. This finding confirmed the 'minimal' influence of $NaPF_6$ and G2 decomposition on the SEI.

Understanding established from thermodynamic computation and experiment suggests that the CEI is more significant in stable cycling. Under a high rate of 2C the SEI exhibited relatively high stability and there was an increase in impedance and CEI thickening. Given that the oxidative stability of ether-based electrolytes is week, this important correlation evidences a direct influence on cycling stability leading to accumulation of organic constituents within the CEI and weakening its mechanical properties [71]. To obviate this Lu et al. reported a solution *via* incorporation of a size dependent artificial CEI layer [74]. In using a uniform 3.2 Å pore size film achieved *via* 3 A zeolite molecular sieve (3AZMS), aggregate coordination between anions and cations rich regions (characterized by PF_6^- coordination with two sodium ions) was selectively used and thereby differing from conventional solvent-solvation structure (involving a pair of G2 coordination), Fig. 5d. The result was establishment of localized high concentration ether-based electrolyte regions, exhibiting a lower HOMO energy and an expanded stable voltage exceeding 4.0 V. In contrast to conventional electrolytes, the cathode equipped with the 3AZMS membrane exhibited no significant increase in CEI, consequently preserving the integrity of the cathode material and obviating destructive phase transitions. This configuration reportedly consistently maintains a Battery CE > 99.55 %.

The importance of electrolyte and artificial interface modifications is preservation of electrochemical stability at enlarged ESW, and mitigation of irreversible electrolyte decomposition.

Modified current collectors

Because there is no active material to store sodium ions in the anode-free configuration, the current collector is the sole substrate for initial nucleation and further growth of sodium metal during charging. Therefore nucleation and dense growth of sodium metal on the current collector are important to reducing active sodium ion loss and improving cycling life.

The galvanostatic electrodeposition profile, Fig. 6a, presents the potential changes on the current collector during constant

current charge. This is an important reference for studying nucleation and growth. To overcome the energy barrier for initial nucleation on the bare current collector, a higher magnitude of nucleation overpotential results in a'small' pit at the onset of charging curve. The deposition of sodium on the current collector starts from a heterogeneous nucleation after sodium ions penetrate through SEI layer and gain electrons from the current collector [78]. The Gibbs free energy change (Fig. 6a inset) for the heterogeneous nucleation of nuclei with radius R can be described in terms of the bulk free energy and surface free energy and written as:

$$\Delta G = -\frac{4\pi R^3}{3}\Delta G_V + 4\pi R^2\gamma \tag{14}$$

where ΔG_V and γ are Gibbs free energy per volume, and surface energy for the interface between the sodium nuclei and substrate. However, given nucleation is driven by the applied electric field, the Gibbs free energy can be written as:

$$\Delta G = -\frac{4\pi R^3}{3}\left(\Delta G_V + \frac{F\eta}{V_m}\right) + 4\pi R^2\gamma \tag{15}$$

where F, η and V_m are, respectively, Faraday constant, overpotential and molar volume of sodium. The critical radius, the minimum size of an embryo reaches to subsequent growth stage, can be computed from $\partial\Delta G/\partial R = 0$. The nuclei radius can therefore be written as:

$$R_{crit} = \frac{2\gamma V_m}{F\eta} \tag{16}$$

which evidences the relationship of critical size to overpotential and surface energy. Significantly, this agrees well with reported experiment [78].

Higher overpotential and lower surface energy lead to smaller nuclei, resulting in significant side reactions from the enlarged surface area of electrolyte consumption, SEI formation and loss of active sodium ions. Based on this direct means of current collector modification is to introduce a sodiophilic layer on the current collector, whilst another, is to enlarge the surface area by constructing a 3D designed current collector. The former increases surface energy between the substrate and deposited sodium and the latter decreases the local current density, both however increase the critical radius for the nucleation, leading to lessened side reactions to electrolytes. The energy density and cycling performance of AFSBs using modified current collectors is comparatively summarized as Fig. 6b.

The addition of a sodiophilic layer including carbon based materials and metals [92,93] that form alloys with sodium on conventional current collectors are reportedly to boost cycling performance *via* lowering the energy barrier. 3D designed current collector reportedly reduce local current density are beneficial for large nuclei and lessens dendrite growth based on Sand's time model [94–96]. Yang et al. reported a 3D Cu current collector with a submicron skeleton [97]. When applied in anode-free lithium battery, which is similar to AFSBs, the unique structure was reported to suppress dendritic Li growth compared with a planar Cu current collector. However, the lithiophobic nature of Cu remains unchanged and leads to 'dead Li' formation when Cu-foam with significantly greater pore sizes of 170 μm is used as current collector. Therefore sodiophilic materials decorated 3D current collectors exhibit 'better' performance with synergy. For example, Li et al. reported an oxygen-containing carbonized coconut framework (O-CCF) with a tubular structure to boost sodium plating and stripping [91]. The oxygen-containing functional groups promoted sodiophilicity of O-CCF and decreased nucleation overpotential to 9 mV from 74 mV (bare Cu) under a current density of 1 mA cm^{-2}. The anode-free NVP||O-CCF@Cu cell exhibited an initial discharge capacity of 2.37 mAh cm^{-2} and a capacity retention of 96 % for 100 cycles at 1 mA cm^{-2}.

Introducing a sodiophilic layer, or using a 3D designed current collector, or mixing has reportedly been used to improve stability of sodium deposition in the negative electrode. Most reported findings research used pre-cycled or sodium deposited electrodes that, however, might not be practical for scaled-up manufacturing. However, those progresses in extending the cycling lifespan can be considered an important step before AFSBs.

Pre-sodiation or sodium-rich cathode

To compensate for the loss of active sodium ions and achieve a long cycle-life in AFSBs, pre-sodiation has reported advantages. Because a cathode that provides an additional 11.11 % active sodium ions has practical potential to triple cycle-life. Therefore, sodium-rich cathodes or using sodium-rich pre-sodiation agents in anode-free configuration have been tested to extend lifespan and expand application.

Rudola et al. reportedly used R-$Na_2Fe_2[CN]_6$ as sodium-rich cathodes for AFSBs because of a high capacity of 170.8 mAh g^{-1} [76]. The battery reportedly was run a number of cycles at a lower voltage plateau ca. 3.1 V to compensate the active sodium ions loss in SEI formation, leaving upper voltage plateau of 3.3 V to exhibit full capacity in subsequent cycles. Wu et al. reportedly synthesized a sodium-rich $Na_5V_2(PO_4)_3$ (Na5VP) cathode by electrochemical discharging NVP electrode to 0.1 V with sodium chip in a half-cell [98]. A pre-stored, significant amount of active sodium ions in cathode concurrently boosted energy density and increased the cycle-life, Fig. 7a. By cycling the Na5VP electrode in a high and narrowed voltage window of 3.0–3.8 V, AFSBs lifespan was extended further over 300 cycles. Liu et al. reportedly developed a facile and 'fast' method to synthesize sodium-rich NVP cathodes *via* immersing the NVP electrode in sodium biphenyl dimethoxymethane (Na-Bp, DME) solution [99]. Following 30 s treatment the NVP electrode received electrons from BP^- anion and accommodated sodium ions to form sodium-rich $Na_4V_2(PO_4)_3$ (Na4VP) because of the lower reduction potential for Bp/Bp^- of 0.12 V *vs.* Na/Na^+ compared with NVP electrode sodium intercalation potential of 1.65 V *vs.* Na/Na^+. The anode-free full-cell exhibited a high-capacity retention ratio in prolonged cycles, Fig. 7b.

Chemical pre-sodiation appears a practically promising means to boost the cycling life of AFSBs, without importing components other than Na. However, this requires complex steps in an inert, gas-protected environment and is likely to lead to increased cost. For high energy density SIBs, pre-sodiation is necessary to compensate the active sodium ions loss caused by HC anode. Current pre-sodiation relies on implantation of sodium-rich pre-sodiation agents in cathodes including, $Na_2C_2O_4$ [100], Na_2S [101], Na_3P [102] and NaN_3 [22,103]. These materials will likely be practical in AFSBs. However, the inactive byproducts generated during initial charge such as S, P, and N_2/CO_2 gases is likely to impact energy density, cycle-life and safety of AFSBs.

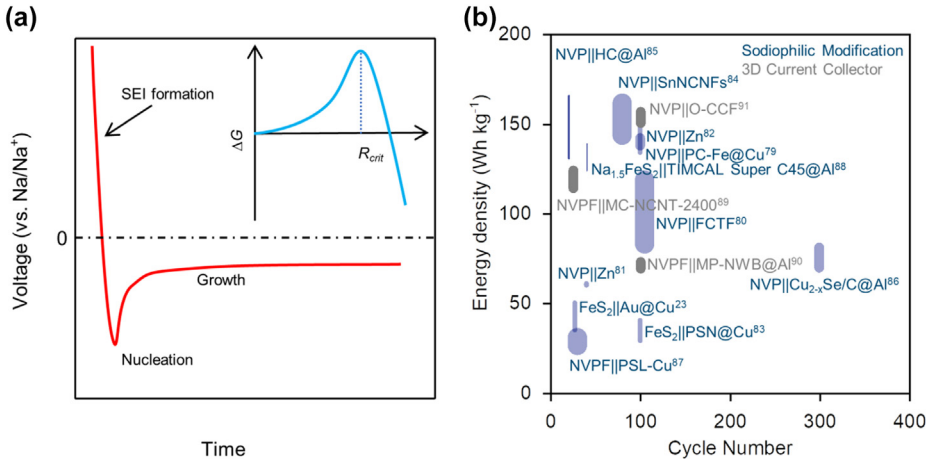


FIG. 6

Developments in current collector modification. (a) Galvanostatic deposition profile for sodium. (Inset: Free Gibbs energy change for heterogeneous nucleation). (b) Energy density and cycling performance for AFSBs using modified current collectors [79–91].

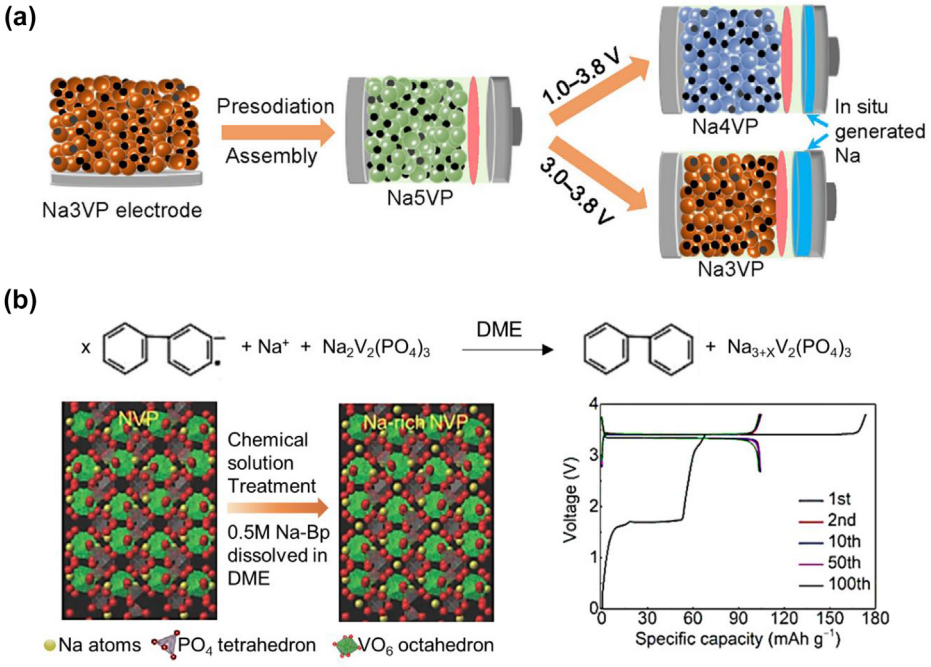


FIG. 7

Illustration of sodium-rich NaxVP electrode. (a) Pre-sodiation with electrochemical method in half-cell and operation of AFSBs cells in two different voltage windows. Reprinted with permission [98] Copyright 2022, Wiley. (b) Pre-sodiation with chemical method and selected galvanostatic curve in a narrowed voltage window. Reprinted with [99] Copyright 2023, Wiley.

Conclusion and perspective

A critical assessment of device energy density, cost, and potential market demand for AFSBs, and comparison with mainstream LIBs and SIBs, together with judicious simulation analyses of cycling life, has found that:

1. AFSBs exhibit high device-level GED from 150 to 270 Wh kg^{-1} and VED from 360 to 640 Wh L^{-1} in 4680 cylindrical battery, comparable to commercial LIBs and therefore making them a practically attractive replacement for LIBs.
2. Cost advantages of AFSBs stem from: (1) Manufacturing, (2) Supply chain management, and (3) Raw material. The material costs per kWh is US$ 48.1, 15.1 % less expensive than commercial NCM||Gr.
3. The combination of competitive energy density and cost is advantageous for AFSBs for electric energy storage, with a potential market share >US$107 billion.
4. A primary limitation in further development of AFSBs is low cycle life that is attributed to limited source of active sodium ions in the AFSBs system, and loss of active sodium ions

caused *via* side reactions. To exhibit a cycle life of >1000 cycles, each cycle will need to exhibit an active sodium ion utilization of >99.965 %.

For future development in AFSBs the following will need to be practically addressed:

1. Cycling performance will need to be improved to permit transition from laboratory-scale to industrial-scale. This will need to be achieved through, (1) Improved, active sodium ions cycling via electrolyte innovation, together with selected additives and anode current collector modification(s), (2) Decreased active sodium ions losses via artificial SEI, and; (3) Increased active sodium ions via use of sodium-rich cathodes, or pre-sodiation.
2. The risks to safety associated with sodium metal in the negative electrode during charging will need to be reduced, most likely through, (1) Development of high-safety separators and separator coatings, (2) Development of flame-retardant electrolyte additives, or use of solid-state electrolytes, and (3) Use of steel shells to boost safety of individual cells, combined together with, (4) Thermal insulation pads to restrict any heat propagation.
3. Production of customized battery components tailored for AFSBs to accommodate volume changes during charge and discharge, and likely achieved through, (1) 3D current collectors with constant thickness, and (2) Custom battery shells in conjunction with a battery manage system to establish constant pressure module.
4. Development of advanced characterizations to establish failure mechanism(s), enabling targeted solutions and optimization(s) of battery chemistry.
5. Development of superior cathode materials with increased energy density and reduced cost to further exploit the advantages of AFSBs.

Driven by the enormous potential market and profits, the AFSBs commercialization will be realized in the near future through combining the above-mentioned methods.

Methods

Device energy density

Design principle is to divide the battery into two components, (1) primary working components, including cathode, anode, electrolyte, separator and current collector, and (2) auxiliary working components, comprising battery shell, current collector disk, and tabs. The concept of 'minimum units' is used to compute the properties of primary working components including, mass, volume and energy. The MUs can be identified as a small area, for example 1 cm^{-2}, composed of cathode current collector, cathode coating (cathode material, binder, and conductive agent), separator, anode coating (anode material, binder, and conductive agent), anode current collector and electrolyte inside the pores of cathode coating, separator and anode coating. Because of the two-side coating in current collectors, the MU encompasses only half of the cathode and anode current collector. Because the volume, mass and energy of MUs are readily computable, and the volume of primary working components in the same battery casing is consistent, the number of the MUs for different materials in a specific battery casing can be established though comparing the volume of MU and the primary working components. Information therefore including, energy, mass and volume of the primary working components can be determined. In the same battery casing, the mass of auxiliary working components remains constant. The device-level energy density for different batteries was with this means computed.

Design of Tesla 4680 battery

The volume, mass and energy parameters for the Tesla 4680 battery are based on test data from first-generation 4680 battery and 25 °C and 1C discharge. When designing minimum unit, information regarding the material type, thickness and porosity of cathode and anode, current collectors, and unit area capacity was determined from open access tear down data. Other information including, the capacity of cathode and anode materials, initial CE and press density were determined from supplier data. The number of minimum units in the primary working components of the 4680 battery was computed *via* dividing the total battery energy by the energy of the minimum unit. The volume of the primary working components in the 4680 battery device was determined by summing volumes for all individual minimum units. The anode volume in the minimal unit is the volume in the charge state. The design accuracy was confirmed by assessing the remaining space inside the device and the total mass of the device.

Design for other battery systems

At the device-level all auxiliary working components remain the same. At the minimum unit level, the separator, binder and conductive agent remain the same. The anode material usage is determined by the capacity of cathode material and anode material together with the N/P ratio. All battery designs have the same positive electrode thickness and porosity, whilst the negative electrode maintains the same porosity as for the Tesla 4680 battery. For all ion batteries, an N/P ratio of 1.1 was used and for anode-free batteries, active ions all come from cathode. The reversible capacity of the ion battery is the smaller one of the reversible active sites on the cathode and the reversible active ions in the whole battery. For anode-free batteries, the reversible capacity is the value of the reversible active sites on the cathode. Anode-free batteries were designed with a theoretical value, 100 % ICE_{ion} and 'dense' deposition. All design and computation were consistent with Tesla 4680 battery.

Material cost(s) and market analysis

The cost for raw materials was sourced from Supplier quotations, London Metal Exchange, and Shanghai Metal Market for August 2023. At material level cost, adjustments were made to specific materials based on practical conditions including, anode to cathode overhang, separator to anode overhang and tabs for current collectors. The market share analysis for different electrochemical energy storage devices was referenced from the 'Electric Vehicle Outlook 2023' and 'Financial Investment Institution Research Report'.

Cycling-life simulation

Just conventional degradation of the battery was simulated. However, the actual degradation mechanisms for batteries are much more complex, for example during cycling, the consumption of the electrolyte can lead to a reduction in the battery lifespan. Additionally, the cycling of a battery is typically controlled *via* charge and discharge voltage, therefore the thickening of the SEI causing an increase in internal resistance can contribute to reduction of battery lifespan. Failures including, short circuits caused by dendrite growth, and active material detachment from the electrode, impact battery lifespan. In any comparison of our model, it is important to rigorously establish that all underlying assumptions are met.

CRediT authorship contribution statement

Yujie Chen: Conceptualization, Data curation, Writing – original draft. **Chao Ye:** Formal analysis, Investigation, Writing – original draft. **Nianji Zhang:** Formal analysis. **Jiahao Liu:** Software. **Huan Li:** Resources, Software. **Kenneth Davey:** Writing – review & editing. **Shi-Zhang Qiao:** Conceptualization, Funding acquisition, Supervision, Writing – review & editing.

Data availability

Data will be made available on request.

Declaration of competing interest

The authors declare that they have no known competing financial interests or personal relationships that could have appeared to influence the work reported in this paper.

Acknowledgements

This work was financially supported by the Australian Research Council (IL230100039, DP220102596, IH200100035, LP210301397 and DE230101011). The authors gratefully acknowledge Chun-Chuan Kao, and Yiran Jiao for helpful discussion(s).

References

[1] M. Li et al., Adv. Mater. 30 (33) (2018) 1800561.
[2] J.M. Turner, Science 376 (6600) (2022) 1361.
[3] C.P. Grey, D.S. Hall, Nat. Commun. 11 (1) (2020) 6279.
[4] R. Schmuch et al., Nat. Energy 3 (4) (2018) 267–278.
[5] X. Sun et al., Mater. Today Energy 14 (2019) 100347.
[6] E.A. Olivetti et al., Joule 1 (2) (2017) 229–243.
[7] J.-Y. Hwang et al., Chem. Soc. Rev. 46 (12) (2017) 3529–3614.
[8] P.K. Nayak et al., Angew. Chem. Int. Ed. 57 (1) (2018) 102–120.
[9] C. Delmas, Adv. Energy Mater. 8 (17) (2018) 1703137.
[10] N. Yabuuchi et al., Chem. Rev. 114 (23) (2014) 11636–11682.
[11] S. Doll, Electrek, 2023. https://electrek.co/2023/06/12/byd-joint-venture-mass-producing sodium-ion-ev-batteries/ (accessed 12 December 2023).
[12] E. Onstad, Reuters, 2021. https://www.reuters.com/business/energy/catls-new-sodium-ion- battery-help-ease-lithium-shortages-2021-08-03/ (accessed 12 December 2023).
[13] C. Randall, Elective, 2023. https://www.electrive.com/2023/02/23/hina-launches-sodium-ion- battery-tests-in-vehicles/ (accessed 12 December 2023).
[14] M. Maisch, PV magazine, 2022. https://www.pv-magazine.com/2022/03/26/the-weekend-read-sodium-ion-batteries-go-mainstream/ (accessed 12 December 2023).
[15] L. Blain, NEW ATLAS, 2022. https://newatlas.com/energy/natron-sodium-ion-battery- production/ (accessed 12 December 2023).
[16] Z. Yang et al., Chem. Rev. 111 (5) (2011) 3577–3613.
[17] H.S. Hirsh et al., Adv. Energy Mater. 10 (32) (2020) 2001274.
[18] T. Yang et al., iScience 26 (3) (2023) 105982.
[19] Q. Ni et al., Batteries 8 (12) (2022) 272.
[20] Y. Li et al., Nat. Energy 7 (6) (2022) 511–519.
[21] Z. Luo et al., Nano Energy 97 (2022) 107203.
[22] J.M. De Ilarduya et al., J. Power Sources 337 (2017) 197–203.
[23] S. Tang et al., Nano Energy 48 (2018) 101–106.
[24] S. Baazouzi et al., Batteries 9 (6) (2023) 309.
[25] J.B. Quinn et al., J. Electrochem. Soc. 165 (14) (2018) A3284–A3291.
[26] J. Liu et al., Next Energy 1 (1) (2023) 100015.
[27] J. Mao et al., Energy Environ. Sci. 15 (7) (2022) 2732–2752.
[28] J. Frazelle, Queue 18 (5) (2020) 5–25.
[29] S. Li et al., Appl. Energy 349 (2023) 121548.
[30] R. Stanek et al., P3 Technol. Rep. P. 3 (2020).
[31] C.S. Ioakimidis et al., Sustainability 11 (9) (2019) 2527.
[32] B. Scrosati, J. Garche, J. Power Sources 195 (9) (2010) 2419–2430.
[33] T. Jin et al., Chem. Soc. Rev. 49 (8) (2020) 2342–2377.
[34] J. Peng et al., Adv. Mater. 34 (15) (2022) 2108384.
[35] R.-M. Gao et al., Energy Storage Mater. 30 (2020) 9–26.
[36] X. Dou et al., Mater. Today 23 (2019) 87–104.
[37] A. Rudola et al., Nat. Energy 8 (3) (2023) 215–218.
[38] S. Mariyappan et al., Chem. Mater. 32 (4) (2020) 1657–1666.
[39] A. Rudola et al., J. Mater. Chem. A 9 (13) (2021) 8279–8302.
[40] Y. Yoda et al., ACS Appl. Mater. Interfaces 10 (13) (2018) 10986–10997.
[41] J. Song et al., J. Am. Chem. Soc. 137 (7) (2015) 2658–2664.
[42] J. Crider, Panasonic To Begin Mass Production of Tesla 4680 Batteries In Fiscal Year April 2023, 2022. https://cleantechnica.com/2022/03/12/panasonic-to-begin-mass-production-of-tesla-4680-batteries-in-fiscal-year-april-2023/ (accessed 12 December 2023).
[43] F. Lambert, LG invests $450 million in producing Tesla's 4680 battery cell format, Electrek, 2022. https://electrek.co/2022/06/14/lg-invests-450-million-iproducing-tesla-4680-battery-cell-format/ (accessed 12 December 2023).
[44] C. Vaalma et al., Nat. Rev. Mater. 3 (4) (2018) 1–11.
[45] T. Liu et al., Energy Environ. Sci. 12 (5) (2019) 1512–1533.
[46] Y. Li et al., Energy Storage Mater. 7 (2017) 130–151.
[47] G. Yingzhe, Cai Xin, 2022. https://www.caixinglobal.com/2022-11-17/amid-eye-wateringlithium-prices-battery-chief-warns-of-overcapacity-101966778.html (accessed 12 December 2023).
[48] Y. Liu et al., iScience 24 (4) (2021) 102332.
[49] W. Yao et al., Electrochem. Energy Rev. 4 (2021) 601–631.
[50] A.M. Boyce et al., ACS Nano 15 (12) (2021) 18624–18632.
[51] F. Duffner et al., Int. J. Prod. Econ. 232 (2021) 107982.
[52] N. Sharmili et al., J. Energy Storage 68 (2023) 107622.
[53] O. Egbue, S. Long, Eng. Manage. J. 24 (3) (2012) 52–62.
[54] S. Althaf, C.W. Babbitt, Resour. Conserv. Recycl. 167 (2021) 105248.
[55] J.T. Frith et al., Nat. Commun. 14 (1) (2023) 420.
[56] N. Kittner et al., Nat. Energy 2 (9) (2017) 1–6.
[57] B. Nef, BloombergNEF, 2021. https://about.bnef.com/blog/battery-pack-prices-fall-to-an average-of-132-kwh-but-rising-commodity-prices-start-to-bite/ (accessed 12 December 2023).
[58] Size of the global battery market from 2018 to 2021, with a forecast through 2030, by technology, Statista, 2023. https://www.statista.com/statistics/1339880/global-battery-market-size-by-technology/ (accessed 12 December 2023).
[59] T. Bashir et al., Energy Mater. 1 (2021) 100019.
[60] Global EV Outlook 2023, IEA, 2023. https://www.iea.org/reports/global-ev-outlook- 2023/trends-in-batteries/ (accessed 12 December 2023).
[61] Electric Vehicle Outlook 2023, BloombergNEF, 2023. https://about.bnef.com/electric-vehicle-outlook/ (accessed 12 December 2023).
[62] Batteries – Thematic Research, GlobalData, 2022. https://www.globaldata.com/store/report/batteries-theme-analysis/ (accessed 12 December 2023).
[63] A. Shao et al., Adv. Energy Sustainability Res. 3 (4) (2022) 2100197.
[64] S. Nanda et al., Adv. Energy Mater. 11 (2) (2021) 2000804.
[65] B.D. Adams et al., Adv. Energy Mater. 8 (7) (2018) 1702097.
[66] J. Xiao et al., Nat. Energy 5 (8) (2020) 561–568.
[67] F. Yang et al., Energy 171 (2019) 1173–1182.
[68] J. Liu et al., Nat. Energy 4 (3) (2019) 180–186.
[69] D. Lin et al., Nat. Chem. 11 (4) (2019) 382–389.
[70] T. Zhang et al., Chem. Rec. 22 (10) (2022) e202200083.
[71] B. Ma et al., Adv. Sci. 8 (12) (2021) 2005006.
[72] Z. Liu et al., ACS Cent. Sci. 9 (6) (2023) 1076–1087.
[73] B. Han et al., Nat. Commun. 12 (1) (2021) 3066.
[74] Z. Lu et al., Angew. Chem. Int. Ed. 61 (20) (2022) e202200410.

[75] C. Wang et al., Adv. Energy Mater. (2023) 2204125.
[76] A. Rudola et al., Electrochem. Commun. 86 (2018) 157–160.
[77] A.W. Tomich et al., Angew. Chem. Int. Ed. 61 (51) (2022) e202208158.
[78] A. Pei et al., Nano Lett. 17 (2) (2017) 1132–1139.
[79] K. Lee et al., Adv. Mater. 34 (14) (2022) 2109767.
[80] R. Zhuang et al., Sci. Adv. 9 (39) (2023) eadh8060.
[81] C. Liu et al., J. Electrochem. Soc. 169 (8) (2022) 080521.
[82] O.J. Dahunsi et al., Nanoscale 15 (7) (2023) 3255–3262.
[83] Q. Chen et al., ACS Appl. Energy Mater. 3 (3) (2020) 2900–2906.
[84] S. Li et al., Adv. Mater. (2023) 2301967.
[85] A.P. Cohn et al., J. Mater. Chem. A 6 (46) (2018) 23875–23884.
[86] H. Li et al., Adv. Energy Mater. 12 (43) (2022) 2202293.
[87] M.E. Lee et al., ACS Appl. Mater. Interfaces 11 (13) (2019) 12401–12407.
[88] A.P. Cohn et al., Nano Lett. 17 (2) (2017) 1296–1301.
[89] H.J. Yoon et al., Adv. Energy Mater. 8 (6) (2018) 1701261.
[90] M.E. Lee et al., Small 15 (37) (2019) 1901274.
[91] T. Li et al., Adv. Energy Mater. 11 (7) (2021) 2003699.
[92] L. Zhang et al., Small 17 (12) (2021) 2007578.
[93] H. Wang et al., J. Mater. Chem. A 7 (41) (2019) 23747–23755.
[94] J.-N. Chazalviel, Phys. Rev. A 42 (12) (1990) 7355–7367.
[95] M. Rosso et al., J. Power Sources 97 (2001) 804–806.
[96] Q. Zhang et al., Inorg. Chem. Front. 5 (4) (2018) 864–869.
[97] C.-P. Yang et al., Nat. Commun. 6 (1) (2015) 8058.
[98] J. Wu et al., InfoMat 4 (4) (2022) e12288.
[99] Y. Liu et al., Adv. Energy Mater. 13 (3) (2023) 2203283.
[100] D. Shanmukaraj et al., ChemSusChem 11 (18) (2018) 3286–3291.
[101] X. Pan et al., Electrochim. Acta 318 (2019) 471–478.
[102] B. Zhang et al., Nat. Commun. 7 (1) (2016) 10308.
[103] G. Singh et al., Electrochem. Commun. 37 (2013) 61–63.